AD_____

AWARD NUMBER: W81XWH-08-1-0234

TITLE: A Mouse Model for In Vivo Detection and Disruption of TGF-beta Signaling in Breast Cancer Metastasis

PRINCIPAL INVESTIGATOR: Manav Korpal

CONTRACTING ORGANIZATION: Princeton University
Princeton, NJ 08544

REPORT DATE: September 2009

TYPE OF REPORT: Annual Summary

PREPARED FOR: U.S. Army Medical Research and Materiel Command
Fort Detrick, Maryland 21702-5012

REPORT DOCUMENTATION PAGE

Form Approved
OMB No. 0704-0188

1. REPORT DATE	**2. REPORT TYPE**	**3. DATES COVERED**
1 September 2009	Annual Summary	1 Sep 2008 – 31 Aug 2009

4. TITLE AND SUBTITLE

A Mouse Model for In Vivo Detection and Disruption of TGF-beta Signaling in Breast Cancer Metastasis

5a. CONTRACT NUMBER

5b. GRANT NUMBER
W81XWH-08-1-0234

5c. PROGRAM ELEMENT NUMBER

6. AUTHOR(S)

Manav Korpal

E-Mail: mkorpal@princeton.edu

5d. PROJECT NUMBER

5e. TASK NUMBER

5f. WORK UNIT NUMBER

7. PERFORMING ORGANIZATION NAME(S) AND ADDRESS(ES)

Princeton University
Princeton, NJ 08544

8. PERFORMING ORGANIZATION REPORT NUMBER

9. SPONSORING / MONITORING AGENCY NAME(S) AND ADDRESS(ES)
U.S. Army Medical Research and Materiel Command
Fort Detrick, Maryland 21702-5012

10. SPONSOR/MONITOR'S ACRONYM(S)

11. SPONSOR/MONITOR'S REPORT NUMBER(S)

12. DISTRIBUTION / AVAILABILITY STATEMENT
Approved for Public Release; Distribution Unlimited

13. SUPPLEMENTARY NOTES

14. ABSTRACT
None provided.

15. SUBJECT TERMS
None provided.

16. SECURITY CLASSIFICATION OF:			**17. LIMITATION OF ABSTRACT**	**18. NUMBER OF PAGES**	**19a. NAME OF RESPONSIBLE PERSON**
a. REPORT	**b. ABSTRACT**	**c. THIS PAGE**			USAMRMC
U	U	U	UU	10	**19b. TELEPHONE NUMBER** *(include area code)*

TECHNICAL REPORTS

nature medicine

Imaging transforming growth factor-β signaling dynamics and therapeutic response in breast cancer bone metastasis

Manav Korpal[1], Jun Yan[1], Xin Lu[1], Shuwa Xu[1], Dorothy A Lerit[1] & Yibin Kang[1,2]

Although the transforming growth factor-β (TGF-β) pathway has been implicated in breast cancer metastasis, its *in vivo* dynamics and temporal-spatial involvement in organ-specific metastasis have not been investigated. Here we engineered a xenograft model system with a conditional control of the TGF-β–SMAD signaling pathway and a dual-luciferase reporter system for tracing both metastatic burden and TGF-β signaling activity *in vivo*. Strong TGF-β signaling in osteolytic bone lesions is suppressed directly by genetic and pharmacological disruption of the TGF-β–SMAD pathway and indirectly by inhibition of osteoclast function with bisphosphonates. Notably, disruption of TGF-β signaling early in metastasis can substantially reduce metastasis burden but becomes less effective when bone lesions are well established. Our *in vivo* system for real-time manipulation and detection of TGF-β signaling provides a proof of principle for using similar strategies to analyze the *in vivo* dynamics of other metastasis-associated signaling pathways and will expedite the development and characterization of therapeutic agents.

Initially identified as a tumor-suppressive cytokine, TGF-β has been recognized as a key mediator of metastasis to bone, lung and other organs[1–8]. However, the *in vivo* dynamics of tumor-stroma interactions mediated by TGF-β signaling during the initiation and progression of metastasis have not been scrutinized. Temporal-spatial variations in TGF-β signaling may determine the differential responses of organ-specific metastases to TGF-β pathway inhibitors and may have major implications for identifying optimal therapeutic windows. TGF-β can be secreted from a wide variety of stromal cells and is often overexpressed by breast cancer cells that have become insensitive to TGF-β growth inhibition[1–4]. Bone is a particularly rich reservoir of the inactive precursor form of TGF-β, which is abundantly produced by osteoblasts and embedded in bone matrix during bone formation and remodeling. TGF-β is thought to be released and activated in the tumor-stroma microenvironment during osteolytic bone metastasis, providing a positive feedback signal from the bone to tumor cells to further stimulate metastasis[9–13]. However, direct evidence for pathological TGF-β signaling *in vivo* is lacking, and the source of TGF-β in bone metastasis has not been thoroughly investigated.

Here we engineered a xenograft system in which we coupled noninvasive quantitative imaging of TGF-β signaling to the conditional control of the TGF-β–SMAD signaling pathway. We monitored the status of TGF-β–SMAD signaling by placing firefly luciferase (F_{LUC}) under the control of a TGF-β–responsive promoter. We used constitutive expression of a *Renilla* luciferase (R_{LUC}) reporter to quantify tumor burden during metastasis development and to additionally serve to normalize F_{LUC} activity to tumor size. In the same cell line, we also engineered an inducible expression system for SMAD4, which allowed *in vivo* conditional manipulation of the TGF-β–SMAD pathway in a stage-specific manner (**Fig. 1a**). This system allowed us to obtain major insights into TGF-β signaling dynamics during metastasis and its response to therapeutic regimens that directly or indirectly disrupt TGF-β signaling *in vivo*.

RESULTS

Engineering and validation of the SCP28-SMAD4^{Tet}Duo system

The MDA-MB-231 human breast cancer cell line produces osteolytic bone metastases when inoculated into nude mice through intracardiac injection (**Supplementary Methods**)[5,14,15]. We chose to use SCP28, a single cell-derived subline of MDA-MB-231, because of its moderate bone and lung metastasis ability and its relative homogeneity[14]. We first engineered the SCP28 cell line to stably express a tetracycline-dependent transcriptional activator (tTA) (**Supplementary Fig. 1**). Next, we stably expressed a short hairpin RNA (shRNA) against the *SMAD4* messenger RNA to suppress endogenous *SMAD4*. We then expressed a complementary DNA encoding a Flag epitope–tagged human SMAD4 from a promoter harboring multiple tetracycline responsive elements (TREs) so that SMAD4 can be replenished in the absence of doxycycline (an analog of tetracycline). We further engineered the cell line to express R_{LUC} under a constitutively active cytomegalovirus (CMV) promoter, allowing quantitative measurement of metastatic tumor burden *in vivo* through noninvasive bioluminescence imaging using coelanterazine as the substrate (**Supplementary Fig. 2a–c**). Finally, we expressed F_{LUC} in these cells under the control of a promoter containing multiple SMAD-binding

[1]Department of Molecular Biology, Princeton University, Princeton, New Jersey, USA. [2]Breast Cancer Program, The Cancer Institute of New Jersey, New Brunswick, New Jersey, USA. Correspondence should be addressed to Y.K. (ykang@princeton.edu).

Received 9 August 2008; accepted 10 February 2009; published online 13 July 2009; doi:10.1038/nm.1943

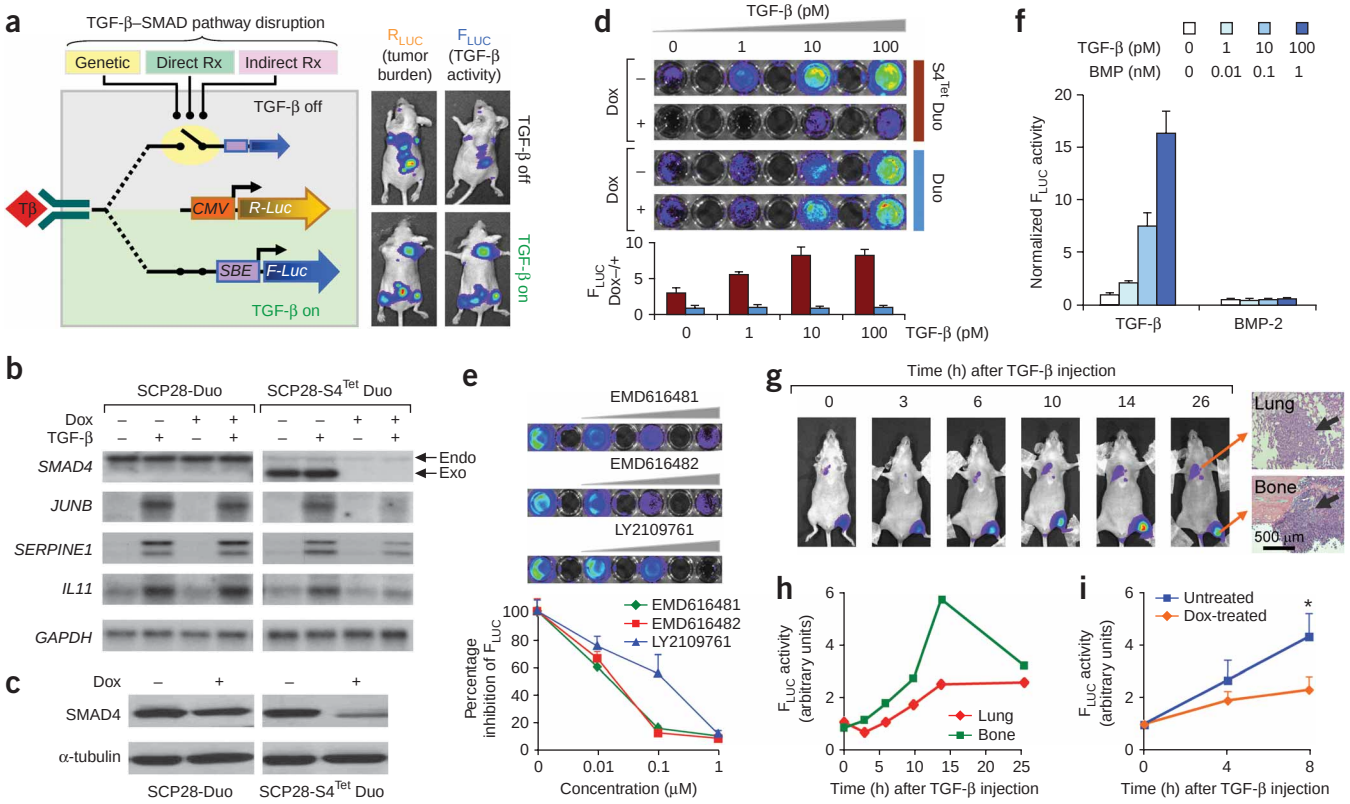

Figure 1 *In vitro* and *in vivo* characterization of the SCP28-SMAD4^{Tet} Duo system. (**a**) A schematic illustration of the system. Rx, pharmalogical inhibitors. (**b**) Northern blot analysis of endogenous (Endo) and exogenous (Exo) *SMAD4* transcripts and TGF-β pathway downstream genes that encode JUNB, SERPINE1 and IL11 in the SCP28-S4^{Tet}Duo cell line and the control SCP28-Duo cell line with or without doxycycline or TGF-β treatments. (**c**) Western blot analysis of SMAD4 protein abundance. (**d**) *In vitro* F_{LUC} response to increasing concentrations of TGF-β with or without doxycycline administration in SCP28-S4^{Tet}Duo and the control SCP28-Duo cell lines. F_{LUC} expression data is also presented as the ratio of the untreated versus doxycycline-treated conditions (Dox−/+) at the bottom. Data represent the means ± s.e.m. of three replicates and were normalized to R_{LUC} expression. (**e**) F_{LUC} activity (in the presence of 100 pM TGF-β) after 24 h treatment by TGF-β receptor I kinase inhibitors (EMD616481, EMD616482 and LY2109761). Data in the bottom graph represent the mean ± s.e.m. of three replicates. (**f**) The F_{LUC} reporter activity in SCP28-S4^{Tet}Duo in response to TGF-β or BMP treatments. Data represent the means ± s.e.m. of three replicates. (**g**,**h**) F_{LUC} reporter response to intravenous injection of recombinant TGF-β in a mouse harboring a pulmonary metastasis and a bone lesion (produced by intracardiac injection of SCP28-S4^{Tet}Duo). Metastatic lesions in lung and bone (arrows) are shown by H&E staining. (**i**) F_{LUC} response to TGF-β in mice with or without doxycycline treatment for 3 d before TGF-β administration ($n = 6$). $^*P < 0.05$ based on a two-sided Wilcoxon rank test. Error bars indicate s.e.m.

elements (SBEs)[16]. Thus, the strength of TGF-β signaling activity in tumor cells is indicated by F_{LUC} bioluminescence imaging using D-luciferin as substrate. We did not detect cross-reactivity of R_{LUC} and F_{LUC} to D-luciferin and coelanterazine, respectively (**Supplementary Fig. 2d**). The dual-imaging system allows the direct comparison of TGF-β signaling activity of tumors with various sizes through the normalization of F_{LUC} activity (absolute TGF-β signaling strength) to R_{LUC} intensity (tumor size). In total, we stably integrated five distinct constructs into SCP28 to create the subline SCP28-SMAD4^{Tet}Duo. We also created a control cell line lacking the inducible expression of SMAD4, SCP28-Duo, for control experiments. Both cell lines showed metastatic ability comparable to the parental SCP28 (**Supplementary Fig. 2e**).

We first confirmed the doxycycline-dependent control of SMAD4 expression and TGF-β pathway activity in the SCP28-SMAD4^{Tet}Duo cell line by *in vitro* experiments (**Fig. 1b**,**c**). TGF-β enhances F_{LUC} activity in both SCP28-Duo and SCP28-SMAD4^{Tet}Duo in a dose-dependent manner (**Fig. 1d**). Such activation is greatly decreased when SCP28-SMAD4^{Tet}Duo cells are cultured in the presence of doxycycline, whereas SCP28-Duo cells are insensitive to such treatment (**Fig. 1d**). Furthermore, administration of three different TGF-β receptor I kinase inhibitors (EMD616481, EMD616482 and LY2109761) caused a dose-dependent decrease of F_{LUC} activity (**Fig. 1e**). Consistent with an earlier report[17], the SBE-F_{LUC} reporter is highly specific for TGF-β, as bone morphogenic protein-2, another member of the TGF-β superfamily, did not activate F_{LUC} in SCP28-SMAD4^{Tet}Duo cells (**Fig. 1f**).

We further confirmed the conditional control of SMAD4 activity and the responsiveness of F_{LUC} to TGF-β in the SCP28-SMAD4^{Tet}Duo system by functional bioluminescence imaging of metastatic lesions *in vivo* (**Fig. 1g–i**). Tail vein injection of TGF-β rapidly enhanced F_{LUC} activity in metastatic lesions within 14 h (**Fig. 1g**,**h**). We confirmed the sensitivity of F_{LUC} activity to the inhibition of SMAD4 expression *in vivo* by bioluminescence imaging of bone lesions in doxycycline-treated and untreated mice harboring bone lesions after TGF-β injection (**Fig. 1i**).

Temporal dependency of bone metastasis on TGF-β–SMAD

To elucidate the temporal dependence of bone metastatic lesions on TGF-β–SMAD signaling, we manipulated TGF-β–SMAD pathway activity in tumor cells *in vivo* at various time points before or after the inoculation of tumor cells. As determined by R_{LUC}

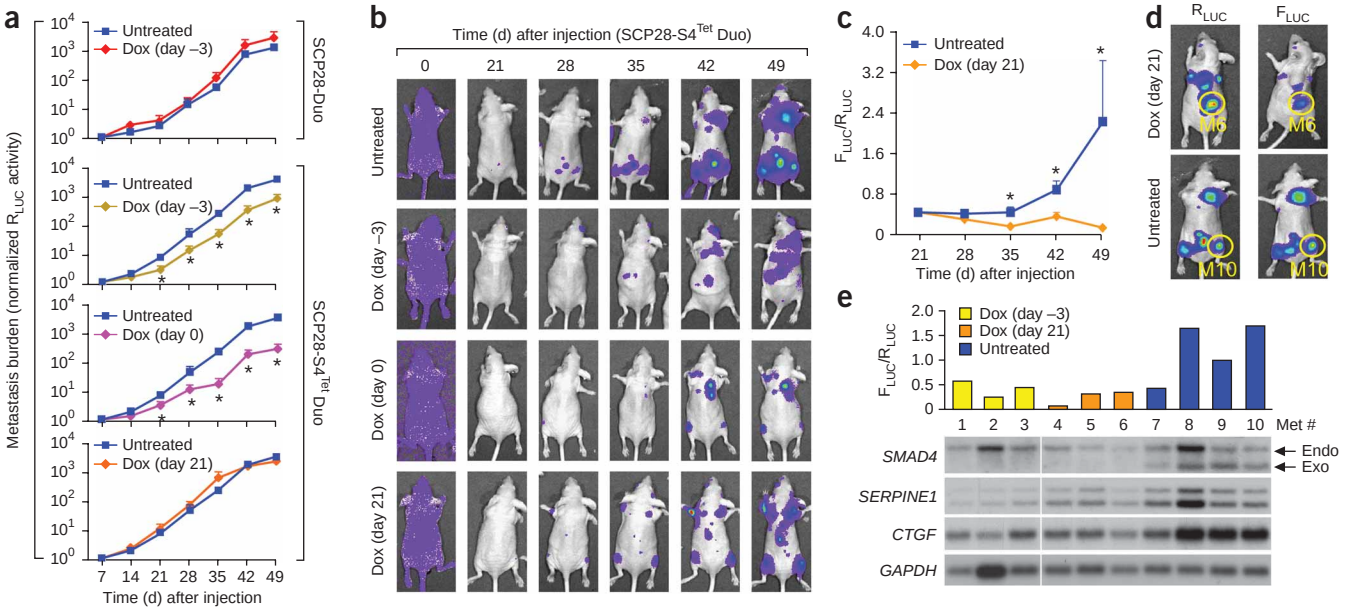

Figure 2 Temporal dependence of bone metastasis on the TGF-β–SMAD pathway *in vivo*. (**a**) Normalized bioluminescence imaging signal curve depicting the intensity of bone metastases (R_{LUC}) developed by intracardiac injection of the control SCP28-Duo cell line or the SCP28-SMAD4^{Tet}Duo cell line using various treatment conditions: untreated (nonmedicated water), treatment initiated 3 d before tumor inoculation (Dox (day −3)), treatment initiated at the time of inoculation (Dox (day 0)) and treatment initiated after metastases become visible by bioluminescence imaging of R_{LUC} (Dox (day 21)). Data are presented as fold change in R_{LUC} at day *n* compared to R_{LUC} photon flux at day 7 (R_{LUC} day *n* / R_{LUC} day 7). $n = 6$ mice per group.*$P < 0.05$ by two-sided Student's *t* test. $P < 0.05$ by analysis of variance (ANOVA) when Dox (day −3) and Dox (day 0) curves were compared with the untreated curve individually (middle two graphs). Error bars indicate s.e.m. (**b**) Representative weekly bioluminescence imaging of R_{LUC} of mice from four experimental groups of mice injected with SCP28-SMAD4^{Tet}Duo. (**c**) Normalized F_{LUC} activity of bone lesions plotted for untreated and Dox (day 21) mice. $n = 6$. Normalized F_{LUC} is calculated as F_{LUC} day *n* / R_{LUC} day *n*. *$P < 0.05$ with a two-sided Student's *t* test. $P < 0.01$ with ANOVA. Error bars indicate s.e.m. (**d**) Representative bioluminescence imaging images from each group. (**e**) Total RNA was extracted from lesions from Dox (day −3), Dox (day 21) and untreated groups and subjected to northern blot analysis with the indicated probes.

bioluminescence imaging, doxycycline treatment of mice injected with the control SCP28-Duo subline did not affect metastasis progression (**Fig. 2a**). In contrast, the SCP28-SMAD4^{Tet}Duo subline pretreated with doxycycline 3 d before inoculation or treated at the time of inoculation (day 0) significantly lowered the number of bone metastases and their rate of progression (**Fig. 2a**,**b** and **Supplementary Fig. 3a**). *SMAD4* knockdown did not affect the growth rate of cells in culture or subcutaneous tumors *in vivo* (data not shown).

To test the role of the TGF-β–SMAD pathway in the continued growth of bone macrometastasis, we delayed doxycycline administration until the detection of bone lesions, usually at day 21. We performed weekly F_{LUC} bioluminescence imaging and normalized it against R_{LUC} activity to account for increases in F_{LUC} signal due to tumor growth. Progression of normalized F_{LUC} activity was significantly lower in lesions from mice given doxycycline at day 21 as compared to those from untreated mice, indicating suppression of TGF-β–SMAD activity (**Fig. 2c**,**d**). However, disruption of the TGF-β–SMAD pathway in these established macrometastases (those at day 21) did not markedly affect the rate of tumor growth (**Fig. 2a**,**b**), suggesting that the TGF-β–SMAD pathway may be crucial for the initial establishment of bone metastasis but is less essential for the maintenance or progression of established macrometastases. Doxycycline administration did not substantially affect normalized F_{LUC} activity in lesions derived from the control SCP28-Duo line (**Supplementary Fig. 4**).

To further define the temporal dependence of bone metastasis on the TGF-β–SMAD pathway, we initiated doxycycline administration in weekly intervals after day 7. Mice pretreated with doxycycline 3 d before tumor inoculation and mice given doxycycline at day 7 showed reduced bone metastasis burden (**Supplementary Fig. 5a**,**b**). However, mice given doxycycline at day 14 and at day 21 showed tumor burdens comparable to those of the solvent-treated group, although normalized F_{LUC} activity was lower in the lesions from mice given doxycycline at days 14 and 21, suggesting successful disruption of the TGF-β–SMAD pathway (**Supplementary Fig. 5c**). Thus, these results suggest that disruption of TGF-β signaling may have the most effective therapeutic response when applied in an adjuvant setting or before metastatic lesions become well established.

To characterize the degree to which F_{LUC} bioluminescence imaging reflects the status of TGF-β–SMAD pathway activity *in vivo*, we extracted total RNA from metastatic lesions and subjected the samples to northern blot analysis (**Fig. 2e**). Lesions isolated from untreated mice (samples 8–10) expressed high levels of exogenous *SMAD4*, whereas those from pretreated mice (samples 1–3) and mice given doxycycline at day 21 (samples 4–6) expressed nearly undetectable levels of exogenous *SMAD4*. Sample 7, the only untreated group sample with low normalized F_{LUC} activity, expressed a much lower amount of exogenous *SMAD4* as compared to other untreated samples (**Fig. 2e**). Furthermore, lesions with high normalized F_{LUC} activity expressed high levels of TGF-β downstream target genes (**Fig. 2e**). These results further confirmed the genetic control of SMAD4 *in vivo* by doxycycline and the strict correlation of SMAD4 function with F_{LUC} activity.

Response to TGF-β receptor inhibitor and bisphosphonates

Having established the reliability of the dual reporter system for real-time quantitative detection of TGF-β–SMAD activity during metastasis, we used it to assess the *in vivo* therapeutic effect of LY2109761,

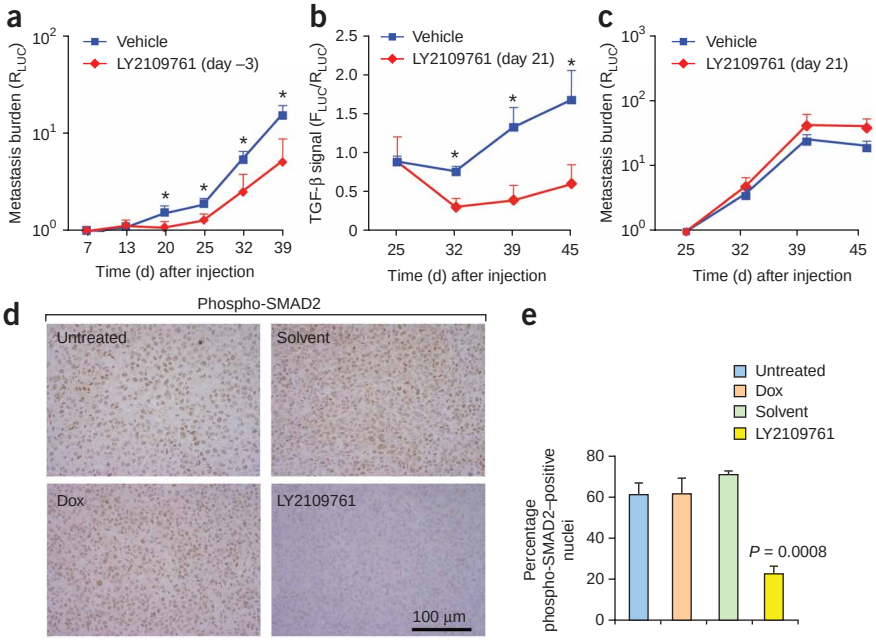

Figure 3 Therapeutic response of bone metastasis to TGF-β receptor I kinase inhibitor LY2109761. (**a**) R_{LUC} bioluminescence imaging analysis of metastasis burden in mice treated with ($n = 11$) or without ($n = 10$) LY2109761 using drug administration starting 3 d before tumor inoculation and continued throughout the course of the study. (**b**) Normalized F_{LUC} activity in lesions from mice treated with ($n = 6$) or without ($n = 8$) LY2109761 using drug administration initiated at day 21 after detection of established bone metastasis. (**c**) R_{LUC} bioluminescence imaging analysis of metastasis burden in mice treated with or without LY2109761 treatment using drug administration initiated at day 21. Data are presented as fold change in R_{LUC} at day n compared to R_{LUC} photon flux at day 25 (R_{LUC} day n / R_{LUC} day 25). In **a**–**c**, $^*P < 0.05$ by two-sided Student's t test. $P < 0.05$ by ANOVA in **a** and **b**. Error bars indicate s.e.m. (**d**,**e**) Representative images and quantification of percentage of cells showing positive nuclear immunohistochemical staining of phospho-SMAD2 in tumor tissue from untreated, solvent-treated, doxycycline-treated and LY2109761-treated mice. Data represent average of four tumors in each group ± s.e.m.

a TGF-β receptor I kinase inhibitor that has been shown to have antimetastasis activities in preclinical testing[18,19]. Treatment of metastatic lesions produced by SCP28-SMAD4^{Tet}Duo cells with LY2109761 led to a decrease in baseline F_{LUC} signaling and its response to intravenous injection of TGF-β (**Supplementary Fig. 6**). Application of the preventative protocol resulted in a significant reduction in the number of bone lesions (**Supplementary Fig. 3b**) and in the progression of bone metastasis burden (**Fig. 3a**). Application of the treatment protocol—twice daily administration of LY2109761 after day 21—suppressed the increase in normalized F_{LUC} activity, thereby indicating the effectiveness of LY2109761 in inhibiting TGF-β signaling *in vivo* (**Fig. 3b**). However, the growth of metastatic lesions was not markedly affected in the treatment protocol (**Fig. 3c**). This observation is consistent with results from the doxycycline treatment experiment, suggesting that inhibition of TGF-β–SMAD signaling may not be sufficient to lower tumor burden in well established bone macrometastases. In agreement with the F_{LUC} reporter analysis, immunohistochemical analysis revealed a decrease in the percentage of phospho-SMAD2–positive nuclei, from 72% to 23%, in mice treated with LY2109761 (**Fig. 3d**,**e**). Doxycycline treatment did not affect SMAD2 phosphorylation (**Fig. 3d**,**e**).

Bisphosphonates are the only currently available palliative treatment to alleviate skeletal-related symptoms in patients with cancer. Administration of the bisphosphonate pamidronate by the preventive protocol (treatment prior to tumor cell inoculation) markedly reduced skeletal morbidity, including a decrease in the number of bone metastases (**Supplementary Fig. 3c**) and delayed progression of metastasis burden (**Fig. 4a**). We also applied the treatment protocol (pamidronate at day 21) and monitored bioluminescence imaging of F_{LUC} to assess TGF-β pathway activity in bone lesions. Pamidronate significantly suppressed the increased normalized F_{LUC} activity in bone lesions (**Fig. 4b**). In contrast, treatment of SCP28-SMAD4^{Tet}Duo cells with pamidronate *in vitro* did not have any influence on R_{LUC} or F_{LUC} activity (**Fig. 4c**). Notably, although pamidronate lowered TGF-β pathway activity in established lesions, the progression of these lesions remained unaffected (**Fig. 4d**). These results suggest that pamidronate indirectly regulates the TGF-β–SMAD pathway activity *in vivo*. We obtained similar results when we treated mice with zoledronic acid, a third-generation bisphosphonate (data not shown).

Bone matrix as a major source of TGF-β in metastasis

Bisphosphonates are thought to reduce the bioavailability of TGF-β to tumor cells through blocking the destruction of bone matrix by osteoclasts[20]. However, to our knowledge, this hypothesis has not been rigorously tested *in vivo*. X-ray radiography of mice treated with bisphosphonates showed little destruction of bone matrix even in bones harboring bioluminescence imaging–detectable metastases (**Fig. 4e** and **Supplementary Fig. 7a**). In contrast, we observed extensive osteolysis in bone lesions in vehicle-treated mice, consistent with significantly higher F_{LUC} activity ($P < 0.05$; **Supplementary Fig. 7b**). Histological staining for tartrate-resistant acid phosphatase (TRAP) activity, a marker of osteoclasts, revealed a significantly lower number of TRAP$^+$ osteoclasts as a result of bisphosphonate treatment ($P < 0.01$; **Fig. 4e**,**f**). Consistent with the bioluminescence imaging analysis of F_{LUC} activity, bisphophonate-treated bone metastases showed a reduction in percentage of phospho-SMAD2–positive nuclei, from 70% to 38% (**Fig. 5a**,**b**), suggesting that the bioavailability of active TGF-β was indeed lower in bisphosphonate-treated mice. Of note, phospho-SMAD2 staining showed a gradient pattern in bone metastasis, with the strongest staining near the tumor-bone interface (**Supplementary Fig. 8a**,**b**). Such a gradient covered a distance of more than 500 μm in bone lesions in the vehicle-treated group, but less than 100 μm in the bisphosphonate-treated group (**Supplementary Fig. 8a**,**b**).

In mice that developed both osteolytic and nonosteolytic bone metastases, osteolytic lesions consistently showed higher normalized F_{LUC} activity than non-osteolytic lesions, regardless of the timing of their initial appearance in the *in vivo* metastasis assay (**Fig. 5c** and **Supplementary Fig. 9**). Furthermore, a rapid increase of TGF-β signaling activity often coincided with the detection of osteolysis by X-ray imaging (**Fig. 5c**). When we compared the intensities of TGF-β

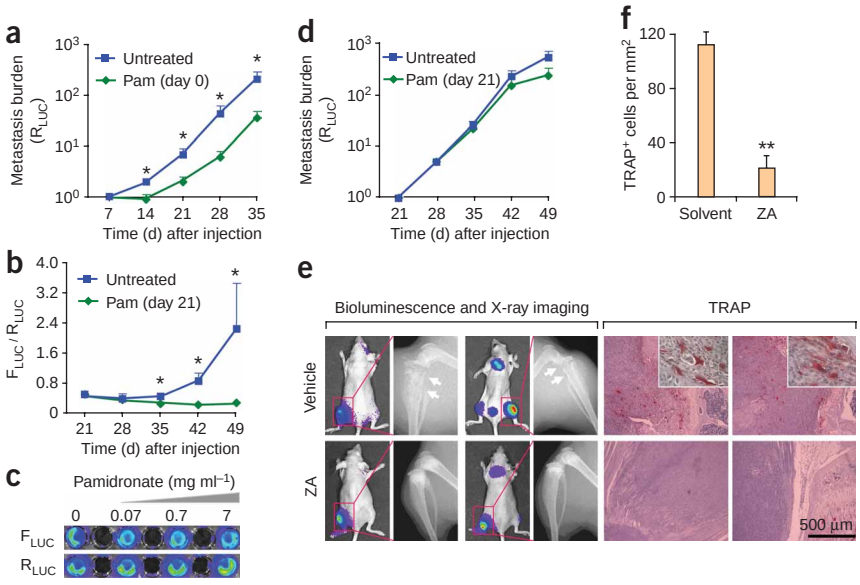

Figure 4 Pamidronate treatment substantially reduces skeletal morbidity and TGF-β signaling activity in metastatic bone lesions. (**a**) R_{LUC} bioluminescence imaging analysis of bone lesions in mice with or without treatment of pamidronate (Pam, at day 0) ($n = 6$ for each condition). Control mice were given saline. (**b**) Normalized F_{LUC} activity of bone lesions in mice harboring established bone lesions with or without pamidronate treatment at day 21. $n = 6$. In **a** and **b**, $^*P < 0.05$ by two-sided Student's t test. $P < 0.01$ by ANOVA. Error bars indicate s.e.m. (**c**) *In vitro* R_{LUC} and F_{LUC} bioluminescence imaging in the presence of 100 pM TGF-β and increasing concentrations of pamidronate. (**d**) R_{LUC} bioluminescence imaging analysis of established bone lesions in mice with or without treatment with pamidronate treatment at day 21, $n = 6$. Error bars indicate s.e.m. (**e**) Bioluminescence imaging and X-ray images, as well as TRAP staining of bone metastases from representative vehicle-treated and zoledronic acid (ZA)-treated mice. Arrows indicate areas of osteolysis. Insets show enlarged images of TRAP$^+$ osteoclasts (at a tenfold magnification). (**f**) The number of TRAP$^+$ cells per mm^2 of tumor adjacent to bone in bone metastases from ZA-treated mice ($n = 8$ lesions) relative to vehicle-treated mice ($n = 7$ lesions). $^{**}P < 0.05$ by two-sided Student's t test. Error bars indicate s.e.m.

signaling activity in metastatic lesions in various organ sites, bone metastases showed a higher normalized F_{LUC} activity as compared to lung metastases (**Supplementary Fig. 10**). Overall, these results support the notion that osteolytic destruction of the bone matrix is a major source of TGF-β during bone metastasis[12].

DISCUSSION

How to sensitively and noninvasively probe the complex signaling network between tumor cells and the host tissue microenvironment has been a major challenge in developing targeted therapeutics for metastatic diseases. Constitutive genetic manipulation of candidate metastasis genes in animal models sidesteps the key question of whether a metastasis gene is essential for the initiation or maintenance of metastasis. Furthermore, histological analysis of metastasis lesions represents static snapshots that often fall short of providing a dynamic view of the key signaling events during the progression or therapeutic intervention of metastasis. In recent years, application of non-invasive imaging technologies has facilitated metastasis research by allowing real-time monitoring of metastasis burdens[21,22]. Here we coupled advanced *in vivo* dual bioluminescence imaging with a xenograft metastasis model in which the TGF-β signaling pathway can be conditionally disrupted by various genetic and pharmacological methods. This powerful platform enabled us to investigate the functional dynamics of the TGF-β pathway in breast cancer metastasis at an unprecedented level.

We validated the responsiveness and specificity of the SBE-F_{LUC} reporter to the TGF-β–SMAD pathway activity by a variety of approaches, including inducible SMAD4 expression and pharmacological

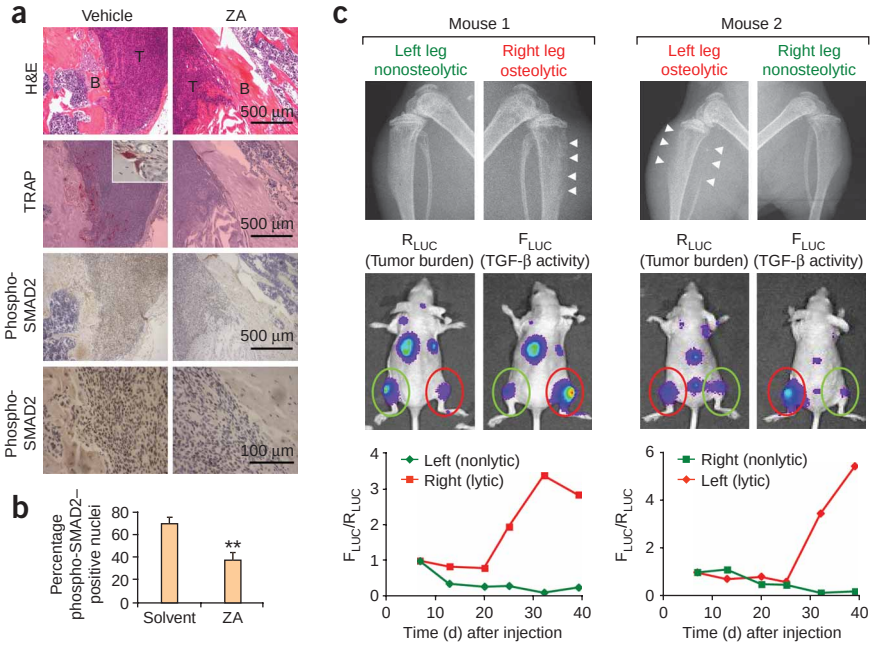

Figure 5 Tumor-induced osteolysis enhances TGF-β signaling in tumor cells. (**a**) H&E, TRAP and phospho-SMAD2 staining of bone lesions in vehicle-treated (saline) and ZA-treated mice. Inset shows enlarged images of TRAP$^+$ osteoclasts. B, bone; T, tumor. (**b**) Quantification of percentage of cells staining positive for nuclear phospho-SMAD2 in saline-treated ($n = 6$) and ZA-treated ($n = 5$) tumors. $^{**}P = 0.004$ by two-sided Student's t test. Error bars indicate s.e.m. (**c**) Tumor-induced osteolysis enhances signaling activity of the TGF-β pathway in tumor cells *in vivo*. Osteolytic lesion in the right leg (mouse 1) or in left leg (mouse 2) induces marked bone destruction of the tibia and fibula (indicated by white arrow heads), resulting in enhanced TGF-β signaling activity as indicated by increasing normalized F_{LUC} activity (bottom graph). In contrast, nonosteolytic lesions at comparable sites on opposite legs show little sign of bone destruction and persistent low level of TGF-β signaling activity.

inhibition of the TGF-β receptor. SBE-F_{LUC} sensitively responds within hours to TGF-β pathway activation or inhibition and allows repetitive, noninvasive and longitudinal studies of TGF-β activity *in vivo*. The use of a constitutively active CMV-R_{LUC} reporter not only allows for simultaneous quantification of the metastasis tumor burden but also serves as an integrated internal control for the normalization of the SBE-F_{LUC} reporter activity. We have found significant correlations between histomorphometric and X-ray measurements of tumor burden with R_{LUC} bioluminescence imaging activity in bone lesions (**Supplementary Fig. 2a–c**). Combination of bioluminescence imaging with other noninvasive imaging modalities, such as positron emission tomography, computed tomography or far-red fluorescent protein imaging by using fusion reporters may further improve the accuracy of real-time quantitative measurement of tumor burden[23–25].

TGF-β activity can be detected in metastases to bone, lung, brain and other organs, with the strongest activity found in the bone metastases. Several lines of evidence from this study experimentally validate the model that osteolytic destruction of bone matrix releases TGF-β to activate a feedback signaling pathway in tumor cells. First, normalized TGF-β signal intensifies in parallel with the progression of osteolytic bone metastasis; second, TGF-β signaling activity is higher in osteolytic bone lesions compared to nonosteolytic lesions; third, when osteolysis is inhibited by bisphosphonates, TGF-β signaling intensity and phospho-SMAD2 staining are markedly lower in bone metastasis; and fourth, a gradient of phospho-SMAD2 staining can be observed at the tumor-bone interface with the highest staining near bone, further suggesting bone as a source of bioactive TGF-β. Therefore, reducing the bioavailability of TGF-β from bone matrix should be an effective strategy for indirectly blocking TGF-β signaling in bone metastasis.

By coupling time-lapse dual-bioluminescence imaging during the course of metastasis development with genetic or pharmacologic manipulation of the TGF-β–SMAD pathway, we were able to monitor the stage-specific functional importance of this pathway during metastasis. We used three distinct methods to disrupt TGF-β–SMAD signaling in bone metastasis. Conditional silencing of SMAD4 expression specifically inhibits the SMAD-dependent pathway downstream of receptor activation. We used a small molecule inhibitor of the TGF-β receptor I kinase, LY2109761, to target the pathway at the level of receptor activation. The third method of TGF-β pathway disruption used bisphosphonates. Although bisphosphonates do not affect the TGF-β pathway directly *in vitro*, they can substantially inhibit TGF-β signaling in *vivo*, presumably through blocking the release of TGF-β from bone matrix by decreasing the activity of osteoclasts. Disruption of the TGF-β signaling pathway by these three methods using a preventive protocol markedly reduced the progression of bone metastasis, suggesting that the TGF-β pathway indeed has a crucial role in promoting bone metastasis. To our surprise, disruption of TGF-β signaling using the treatment protocol consistently became less effective in reducing the tumor burden in well established bone metastases, even though the SBE-F_{LUC} reporter continued to respond well to the treatments. This is in contrast to previous preclinical and clinical studies suggesting that bisphosphonates can substantially reduce skeletal-related events *in vivo*, even in well established metastases[26,27]. This discrepancy may partially be accounted for by the relatively limited time frame of our *in vivo* experiments due to the morbidity of the mice and the several methods used to measure bone metastasis end points. Previous studies assessing the effects of bisphosphonates *in vivo* often relied upon observations of skeletal-related events or radiographic analysis to indirectly measure tumor burden. In contrast, our study applied bioluminescence imaging to directly assess tumor burden. Thus, it is possible that well established bone lesions may become less dependent on bone destruction and TGF-β signaling and, as a consequence, become less sensitive to TGF-β inhibitors. In support of our observation, two recent studies showed that late administration of bisphosphonates was less effective than early administration[28,29]. Furthermore, in clinical trials, pamidronate treatment yields greatest clinical benefit for patients with slowly progressive disease, whereas those patients with advanced skeletal lesions respond poorly, even at high doses[30]. These data argue for the application of direct and indirect TGF-β inhibitors, including bisphosphonates, in an adjuvant setting, where such treatments may achieve the greatest therapeutic benefits[31,32].

Overall, our *in vivo* system of coupling bioluminescence imaging detection of TGF-β signaling with stage-specific disruption of the pathway during metastasis provides proof of principle for using similar strategies to evaluate the temporal-spatial involvement of other metastasis signaling pathways using clinically relevant animal models. This powerful research platform will accelerate the identification and *in vivo* evaluation of antimetastasis compounds that directly or indirectly target the TGF-β pathway.

METHODS

Methods and any associated references are available in the online version of the paper at http://www.nature.com/naturemedicine/.

Note: Supplementary information is available on the Nature Medicine website.

ACKNOWLEDGMENTS

We thank members of the Kang laboratory for insightful discussions and technical suggestions, J. Yingling (Eli Lilly and Company) for the TGF-β receptor I kinase inhibitor and suggestions for the manuscript, S. Gambhir (Stanford University) for triple-reporter plasmids, R. Agami (The Netherlands Cancer Institute) for pRS-GFP, T. Guise and K. Mohammad for technical advice in bone histology and G. Hu for statistical support. Y.K. is a Champalimaud Investigator funded by a Department of Defense Era of Hope Scholar Award and grants from the American Cancer Society, the Susan G. Komen Foundation and the New Jersey Commission on Cancer Research. M.K. is supported by a predoctoral fellowship from the Department of Defense Breast Cancer Research Program.

AUTHOR CONTRIBUTIONS

Y.K. and M.K. designed experiments. Y.K. supervised experiments. M.K. and J.Y. performed the experiments. M.K., J.Y., X.L., S.X. and D.A.L. contributed to molecular cloning and engineering of cell lines. M.K. and Y.K. wrote the manuscript. All authors discussed the results and commented on the manuscript.

Published online at http://www.nature.com/naturemedicine/.
Reprints and permissions information is available online at http://npg.nature.com/reprintsandpermissions/.

1. Yingling, J.M., Blanchard, K.L. & Sawyer, J.S. Development of TGF-β signalling inhibitors for cancer therapy. *Nat. Rev. Drug Discov.* **3**, 1011–1022 (2004).
2. Bierie, B. & Moses, H.L. Tumour microenvironment: TGF-β: the molecular Jekyll and Hyde of cancer. *Nat. Rev. Cancer* **6**, 506–520 (2006).
3. Dumont, N. & Arteaga, C.L. Targeting the TGF-β signaling network in human neoplasia. *Cancer Cell* **3**, 531–536 (2003).
4. Massagué, J. TGF-β in cancer. *Cell* **134**, 215–230 (2008).
5. Yin, J.J. *et al.* TGF-β signaling blockade inhibits PTHrP secretion by breast cancer cells and bone metastases development. *J. Clin. Invest.* **103**, 197–206 (1999).
6. Padua, D. *et al.* TGF-β primes breast tumors for lung metastasis seeding through angiopoietin-like 4. *Cell* **133**, 66–77 (2008).
7. Kang, Y. *et al.* Breast cancer bone metastasis mediated by the Smad tumor suppressor pathway. *Proc. Natl. Acad. Sci. USA* **102**, 13909–13914 (2005).
8. Muraoka-Cook, R.S. *et al.* Activated type I TGF-β receptor kinase enhances the survival of mammary epithelial cells and accelerates tumor progression. *Oncogene* **25**, 3408–3423 (2006).
9. Mundy, G.R. Metastasis to bone: causes, consequences and therapeutic opportunities. *Nat. Rev. Cancer* **2**, 584–593 (2002).
10. Roodman, G.D. Mechanisms of bone metastasis. *N. Engl. J. Med.* **350**, 1655–1664 (2004).

11. Guise, T.A. *et al.* Molecular mechanisms of breast cancer metastases to bone. *Clin. Breast Cancer* **5**Suppl, S46–S53 (2005).
12. Pfeilschifter, J. & Mundy, G.R. Modulation of type β transforming growth factor activity in bone cultures by osteotropic hormones. *Proc. Natl. Acad. Sci. USA* **84**, 2024–2028 (1987).
13. Dallas, S.L., Rosser, J.L., Mundy, G.R. & Bonewald, L.F. Proteolysis of latent transforming growth factor-β (TGF-β)-binding protein-1 by osteoclasts. A cellular mechanism for release of TGF-β from bone matrix. *J. Biol. Chem.* **277**, 21352–21360 (2002).
14. Kang, Y. *et al.* A multigenic program mediating breast cancer metastasis to bone. *Cancer Cell* **3**, 537–549 (2003).
15. Minn, A.J. *et al.* Distinct organ-specific metastatic potential of individual breast cancer cells and primary tumors. *J. Clin. Invest.* **115**, 44–55 (2005).
16. Zawel, L. *et al.* Human SMAD3 and SMAD4 are sequence-specific transcription activators. *Mol. Cell* **1**, 611–617 (1998).
17. Lin, A.H., Luo, J., Mondshein, L.H., ten Dijke, P., Vivien, D., Contag, C.H. & Wyss-Coray, T. Global analysis of Smad2/3-dependent TGF-β signaling in living mice reveals prominent tissue-specific responses to injury. *J. Immunol.* **175**, 547–554 (2005).
18. Melisi, D. *et al.* LY2109761, a novel transforming growth factor β receptor type I and type II dual inhibitor, as a therapeutic approach to suppressing pancreatic cancer metastasis. *Mol. Cancer Ther.* **7**, 829–840 (2008).
19. Li, H.Y. *et al.* Optimization of a dihydropyrrolopyrazole series of transforming growth factor-β type I receptor kinase domain inhibitors: discovery of an orally bioavailable transforming growth factor-β receptor type I inhibitor as antitumor agent. *J. Med. Chem.* **51**, 2302–2306 (2008).
20. Russell, R.G. *et al.* Bisphosphonates: an update on mechanisms of action and how these relate to clinical efficacy. *Ann. NY Acad. Sci.* **1117**, 209–257 (2007).
21. Gross, S. & Piwnica-Worms, D. Spying on cancer: molecular imaging *in vivo* with genetically encoded reporters. *Cancer Cell* **7**, 5–15 (2005).
22. Gelovani Tjuvajev, J. & Blasberg, R.G. *In vivo* imaging of molecular-genetic targets for cancer therapy. *Cancer Cell* **3**, 327–332 (2003).
23. Deroose, C.M. *et al.* Multimodality imaging of tumor xenografts and metastases in mice with combined small-animal PET, small-animal CT and bioluminescence imaging. *J. Nucl. Med.* **48**, 295–303 (2007).
24. Hoffman, R.M. Imaging cancer dynamics *in vivo* at the tumor and cellular level with fluorescent proteins. *Clin. Exp. Metastasis* **26**, 345–355 (2009).
25. Fritz, V. *et al.* Micro-CT combined with bioluminescence imaging: a dynamic approach to detect early tumor-bone interaction in a tumor osteolysis murine model. *Bone* **40**, 1032–1040 (2007).
26. Body, J.J.D.I., Lichinitzer, M., Lazarev, A., Pecherstorfer, M., Bell, R., Tripathy, D. & Bergstrom, B. Oral ibandronate reduces the risk of skeletal complications in breast cancer patients with metastatic bone disease: results from two randomised, placebo-controlled phase III studies. *Br. J. Cancer* **90**, 1133–1137 (2004).
27. Tripathy, D., Lichinitzer, M., Lazarev, A., MacLachlan, S.A., Apffelstaedt, J., Budde, M., Bergstrom, B. & MF 4434 Study Group. Oral ibandronate for the treatment of metastatic bone disease in breast cancer: efficacy and safety results from a randomized, double-blind, placebo-controlled trial. *Ann. Oncol.* **15**, 743–750 (2004).
28. El-Abdaimi, K. *et al.* Pamidronate prevents the development of skeletal metastasis in nude mice transplanted with human breast cancer cells by reducing tumor burden within bone. *Int. J. Oncol.* **22**, 883–890 (2003).
29. van der Pluijm, G. *et al.* Interference with the microenvironmental support impairs the *de novo* formation of bone metastases *in vivo*. *Cancer Res.* **65**, 7682–7690 (2005).
30. Coleman, R.E., Purohit, O.P., Vinholes, J.J. & Zekri, J. High dose pamidronate. *Cancer* **80**, 1686–1690 (1997).
31. Coleman, R. On the horizon: can bisphosphonates prevent bone metastases? *Breast* **16**Suppl 3, S21–S27 (2007).
32. Diel, I.J. *et al.* Reduction in new metastases in breast cancer with adjuvant clodronate treatment. *N. Engl. J. Med.* **339**, 357–363 (1998).

ONLINE METHODS

Molecular cloning. We generated pMSCV-RFP-R_{LUC} by cloning the coding sequence of a R_{LUC}-mRFP-TK triple fusion protein[33] between the BglII and HpaI sites of pMSCVpuro (BD Clontech). We subsequently removed the puromycin resistance gene expression cassette by restriction digestion of the plasmid by PshA1 and ClaI, followed by ligation of the blunted ends. We generated a TGF-β–responsive F_{LUC} reporter, pSBE-F_{LUC}, by inserting four tandem copies of the consensus SMAD binding site[16] into the BglII site of pTA-Luc-Pur (BD Clontech). We generated pRS-GFP-SMAD4 by cloning the previously reported shRNA sequence targeting the *SMAD4* (5′-GGT GTGCAGTTGGAATGTA-3′)[7] into the pRS-GFP vector[34]. We inserted a cDNA encoding an shRNA-insensitive Flag-SMAD4 (ref. 7) into the XbaI site of the Tet-off expression vector pUHD10-3hygro[35] to generate pUHD10-3hygro-Flag-SMAD4.

Engineering of SCP28-SMAD4^{Tet} Duo and SCP28-Duo. We stably transfected SCP28 cells with a tTA expression plasmid (pUHD15-1-Neo)[35] under G418 selection. Next, we screened transfectants for their responsiveness to doxycycline by transiently transfecting a tetracycline-responsive luciferase reporter pTRE2-Pur-luc (BD Clontech). Clones showing the best doxycycline-regulated expression were further stably transfected with pSBE-F_{LUC} under puromycin selection. We then tested the functional expression of F_{LUC} in response to TGF-β *in vitro* and transduced functional clones with retroviruses produced from pMSCV-RFP-R_{LUC}. We selected RFP-positive cells by FACS. Stable clones without further modification served as the control SCP28-Duo subline. To establish the SCP28-SMAD4^{Tet} Duo subline, we transduced the SCP28-Duo cell line with pRS-GFP-SMAD4 and selected GFP-positive cells by FACS. Finally, we stably transfected the pUHD10-3hygro-Flag-SMAD4 plasmid into the cell line to complete the engineering of SCP28-SMAD4^{Tet} Duo.

Bioluminescent imaging and analysis. For *in vitro* studies, we added native coelenterazine (for R_{LUC} imaging) (Prolume) or D-luciferin (for F_{LUC} imaging) (Caliper LifeScience) directly to cultured cells in medium to a final concentration of 50 μg ml^{-1}. Two minutes later, we measured photon flux with the IVIS 200 bioluminescence imaging system (Caliper Life Sciences). We analyzed data with LIVINGIMAGE software (Caliper Life Sciences). For *in vivo* studies, we injected anesthetized mice retro-orbitally with 1 mg per kg body weight coelenterazine or 75 mg per kg body weight D-luciferin. We acquired bioluminescence images by the IVIS Imaging System. Generally, we staggered weekly imaging of R_{LUC} and F_{LUC} in the same mice by at least 24 h. We performed analysis by measuring photon flux of a region of interest drawn around a bioluminescence signal of a metastasis lesion to be measured. We normalized R_{LUC} signal for each metastatic lesion to R_{LUC} signal obtained at day 7 for the preventative protocol and to day 21 for the treatment protocol. We normalized F_{LUC} signal of bone lesions to R_{LUC} signal of the respective lesions to assess the effect of treatment on TGF-β signaling activity.

Dosing regimens and experimental protocols. All procedures involving mice, such as housing and care, and all experimental protocols were approved by Institutional Animal Care and Use Committee of Princeton University. We used doxycycline hyclate (Sigma) at a concentration of 1 μg ml^{-1} *in vitro*. We used distilled water with 0.5 mg ml^{-1} doxycycline in tinted bottles as drinking water to suppress Flag-SMAD4 expression *in vivo*. We dissolved TGF-β receptor I kinase inhibitors 2-(3-(6-methylpyridin-2-yl)-1H-pyrazol-4-yl)-1,5-naphthyridine (EMD Biosciences catalog number 616452) and (3-(pyridin-2-yl)-4-(4-quinonyl))-1H-pyrazole (LY364947, EMD catalog number 616451) in DMSO for *in vitro* experiments. We dissolved compound LY2109761 (Eli Lilly) at a concentration of 15 g l^{-1} in 1% sodium carboxymethylcellulose, 0.5% sodium lauryl sulfate and 0.05% Antifoam (Eli Lilly). We administered dissolved compound at a dosage of 50 mg per kg body weight twice daily (every 12 h) by gastro-gavaging using sterile 22G 1.5-inch feeding needles (Roboz Surgical Instrument). We administered pamidronate (Novartis), a second-generation nitrogenated bisphosphonate, to mice at a dosage of 5 mg per kg body weight per day subcutaneously, which is equivalent to the current clinical doses approved for the treatment of skeletal metastases. We used zoledronic acid (Novartis), a third-generation nitrogenated bisphosphonate, at a dosage of 250 μg per kg body weight per day subcutaneously. In the preventative protocol, we administered either doxycycline continuously through drinking water of mice beginning 3 d before tumor cell inoculation, compound LY2109761 twice daily beginning on the day of tumor cell inoculation, or bisphosphonates once daily also beginning on the day of tumor inoculation. In the treatment protocol, we administered all inhibitors of the TGF-β pathway after overt lesions became visible by R_{LUC} bioluminescence imaging, usually at day 21.

Statistical analyses. We reported results as means ± s.e.m. We performed two-sided independent Student's *t* test without equal variance assumption or the Wilcoxon signed-rank test to analyze individual time points of bioluminescence imaging data. We used repeated measures ANOVA to assess statistical significance of whole bioluminescence imaging curves, encompassing several time points, between two treatment groups. We performed the two-sided independent Student's *t* test to analyze end points of *in vitro* luciferase assays and histology data.

33. Ray, P., De, A., Min, J.J., Tsien, R.Y. & Gambhir, S.S. Imaging tri-fusion multimodality reporter gene expression in living subjects. *Cancer Res.* **64**, 1323–1330 (2004).
34. Voorhoeve, P.M. & Agami, R. The tumor-suppressive functions of the human INK4A locus. *Cancer Cell* **4**, 311–319 (2003).
35. Reynisdóttir, I., Polyak, K., Iavarone, A. & Massagué, J. Kip/Cip and Ink4 Cdk inhibitors cooperate to induce cell cycle arrest in response to TGF-β. *Genes Dev.* **9**, 1831–1845 (1995).

doi:10.1038/nm.1943